Available online at www.sciencedirect.com

ScienceDirect

Journal of the Chinese Medical Association 81 (2018) 487–495

www.jcma-online.com

Original Article

Characterization and functional correlation of multiple imaging modalities with focal choroidal excavation

Yun-Chen Chen [a], Yu-Bai Chou [b], Cheng-Kuan Lin [c], Chia-Chen Tsai [a], Tsui-Kang Hsu [a], Yu-Fan Chang [b], Hsiao-Ming Chao [a], Tao-Hsin Tung [d,e], Shih-Jen Chen [b,f,*], Jorn-Hon Liu [a]

[a] *Department of Ophthalmology, Cheng Hsin General Hospital, Taipei, Taiwan, ROC*
[b] *Department of Ophthalmology, Taipei Veterans General Hospital, Taipei, Taiwan, ROC*
[c] *Department of Environmental Health, Harvard Chan School of Public Health, Boston, MA, USA*
[d] *Faculty of Public Health, College of Medicine, Fu-Jen Catholic University, Taipei, Taiwan, ROC*
[e] *Department of Medical Research and Education, Cheng Hsin General Hospital, Taipei, Taiwan, ROC*
[f] *School of Medicine, National Yang-Ming University, Taipei, Taiwan, ROC*

Received May 17, 2017; accepted July 28, 2017

Abstract

Background: To investigate the clinical manifestations and imaging features of near-infrared autofluorescence (NIA), infrared reflectance (IR), fundus autofluorescence (FAF), indocyanine green angiography (ICGA) and fluorescein angiography (FAG) in the detection of patients with focal choroidal excavation (FCE) identified by cross-sectional spectral-domain optical coherence tomography (SD-OCT).
Methods: This retrospective cross-sectional study included 12 eyes of 10 Taiwanese patients with FCE diagnosed by SD-OCT. The areas and depths of FCE in serial cross-sectional and en-face OCT were compared in different imaging modalities. NIA, IR, FAF, ICGA and FAG images were obtained. Best corrected visual acuity, subjective distortion area in the Amsler grid and history of maculopathies were also recorded.
Results: In areas where the choroid started to excavate as shown in SD-OCT, hypo-autofluorescence in NIA was noted. The area of hypo-fluorescence in NIA of all the FCE lesions showed good correlation with the size. The area of FCE was associated with complications such as choroidal neovascularization and central serous chorioretinopathy ($p = 0.014$, d.f = 1) and the volume (NIA area × Depth measured by SD-OCT × 1/3) was associated with subjective distortion strongly ($p = 0.051$, Spearman's correlation = 0.600).
Conclusion: Among all image modalities, NIA was the most sensitive tool in area measurement of FCE and peripheral lesion detection. Also, the volume of FCE was associated with subjective distortion and the area was related to complications. Recording the area and volume of FCE could play an important role in monitoring complications.

Keywords: Choroid-retina disease; Focal choroidal excavation; Near-infrared autofluorescence; Spectral-domain optical coherence tomography

1. Introduction

Focal choroidal excavation (FCE), a localized depression of the choroid over the macula, was first identified by time-domain optical coherence tomography (OCT) in 2006,[1] and subsequently in other reports.[2–5] Patients with FCE are generally associated with good visual acuity, mild metamorphopsia or without symptoms. However, FCE has been reported to be accompanied with choroidal neovascularization

Conflicts of interest: The authors declare that they have no conflicts of interest related to the subject matter or materials discussed in this article.

* Corresponding author. Dr. Shih-Jen Chen, Department of Ophthalmology, Taipei Veterans General Hospital, 201, Section 2, Shi-Pai Road, Taipei 112, Taiwan, ROC.
E-mail address: sjchen@vghtpe.gov.tw (S.-J. Chen).

https://doi.org/10.1016/j.jcma.2017.07.017

(CNV) and central serous chorioretinopathy (CSCR),[4,6–10] and it may develop during follow-up in asymptomatic patients.[5] CNV complexes have also been reported to develop within the boundary of the excavation.[10,11] The characteristic morphology of FCE is similar to the findings in patients at high risk of CSCR and CNV.[2] Other retinal conditions including polypoidal choroidal vasculopathy and age-related macular degeneration have also been shown to be associated with FCE.[3,5,12–14] Therefore, patients with FCE should regularly be monitored for the potential development of other retinal diseases.

In most patients, the presence of FCE is not clearly evident on routine clinical examinations. Subtle abnormalities with mild to moderate pigmentary disturbances on fundoscopy have been reported. Invasive imaging modalities such as fluorescein angiography (FAG) show varying degrees of hyper-fluorescence and hypo-fluorescence depending on the level of alteration in retinal pigment epithelium (RPE). Indocyanine green angiography (ICGA) may show hypo-fluorescence at the excavation. Currently, spectral-domain optical coherence tomography (SD-OCT) is used to detect morphologic details of FCE, and it is the most widely used non-invasive tool. However, in cases with bilateral involvement or multiple lesions in one eye,[2–4,15] SD-OCT of the fovea which is confined to the posterior pole may not detect all lesions.

To detect FCE lesions precisely and to monitor the development non-invasively, image tools play an important role. However, associations between the area and volume of FCE, visual acuity, functional status and complications have not been elucidated. Therefore, this study aimed to investigate the clinical manifestations and image features in 10 patients (12 eyes) using near-infrared autofluorescence (NIA), infrared reflectance (IR), fundus autofluorescence (FAF), ICGA and FAG to evaluate FCE confirmed by cross-sectional SD-OCT.

2. Methods

In the cross-sectional study, a total of 13 consecutive Taiwanese patients were identified with FCE at Cheng Hsin General Hospital and Taipei Veterans General Hospital during the period between October 2012 and August 2015. 12 eyes of 10 patients were followed for 3–36 months and included in our research. None of the patients had a history of trauma, posterior uveitis, prior retinal or choroidal infections or surgery. Study protocols were approved by the Institutional Review Board of Cheng Hsin General Hospital.

2.1. Imaging studies

The medical records of the patients were reviewed. The findings of clinical examinations including best-corrected visual acuity (BCVA), refraction, slit-lamp, intraocular pressure (IOP), ophthalmoscopy, fundus photography, FAG, ICGA, SD-OCT, enhanced depth imaging optical coherence tomography (EDI-OCT), multidimensional en-face optical coherence tomography (en-face OCT), FAF, NIA and IR image findings were also reviewed.

FAG and ICGA were performed in five eyes of four patients presenting with CSCR (Figs. 3 and 4) and CNV (Fig. 2) by Heidelberg retinal angiography (HRA; Heidelberg Engineering, Heidelberg, Germany).

The choroidal excavation was detected by SD-OCT (Spectralis HRA-OCT; Heidelberg Engineering, Heidelberg, Germany). The factors investigated by SD-OCT were documented in cone-shaped, bowl-shaped, and mixed types of FCE. Lesions were further subdivided into conforming and non-conforming groups.[6] The conforming group was defined as no separation of the photoreceptor tips and RPE (Figs. 1, 2, and 4), and the non-conforming group was defined where the photoreceptors appeared to be detached from the RPE with an intervening hypo-reflective space (Fig. 3). The depth of each excavation was measured using internal caliper software with images crossing the center of the excavation (Fig. 4). Morphologic characteristics of the retina were analyzed by SD-OCT (Fig. 1) including the retinal nerve fiber layer (RNFL), ganglion cell layer (GCL), inner plexiform layer (IPL), inner nuclear layer (INL), outer plexiform layer (OPL), outer nuclear layer (ONL), external limiting membrane (ELM), myoid zone (MZ), ellipsoid zone (EZ), interdigitation zone (IZ), and the retinal pigment epithelial band (RPE/Bruch's band).

EDI-OCT images were taken to evaluate the choroidal morphologic features, including the shape of the choroidoscleral border, the choriocapillaris (CC), the deeper choroidal vessels (Sattler's and Haller's layer), the choroidal thickness at the deepest portion of the FCE lesion, and the maximal thickness of choroid adjacent to the FCE lesion (Fig. 4). En-face OCT was used to evaluate the characteristics of FCE (Figs. 1 and 4).

FAF (diode laser light, short-wavelength; excitation 486 nm; emission > 500 nm), NIA (diode laser light; excitation 786 nm; emission 800 nm) and IR (diode laser light; excitation 815 nm) images were obtained using a confocal scanning laser ophthalmoscope (SLO) (Heidelberg Engineering Spectralis HRA) and were evaluated by two examiners.

2.2. Clinical manifestations

The complication of FCE such as CNV and CSCR were diagnosed by using SD-OCT and FAG.

2.3. Statistical analysis

The BCVA was converted to the logarithm of the minimal angle of resolution (logMAR) to facilitate a visual comparison and statistical analysis. In the univariate analysis, Mann–Whitney *U* test was calculated for continuous variables. Spearman correlation coefficient method was applied to investigate the relationship between volume, subjective distortion and associated continuous factors. The Kruskal–Wallis test was used to compare the area of FCE to the accompanied complication such as CNV and CSCR. Statistical analysis was performed using SPSS 20.0. A p-value of <0.05 was considered statistically significant.

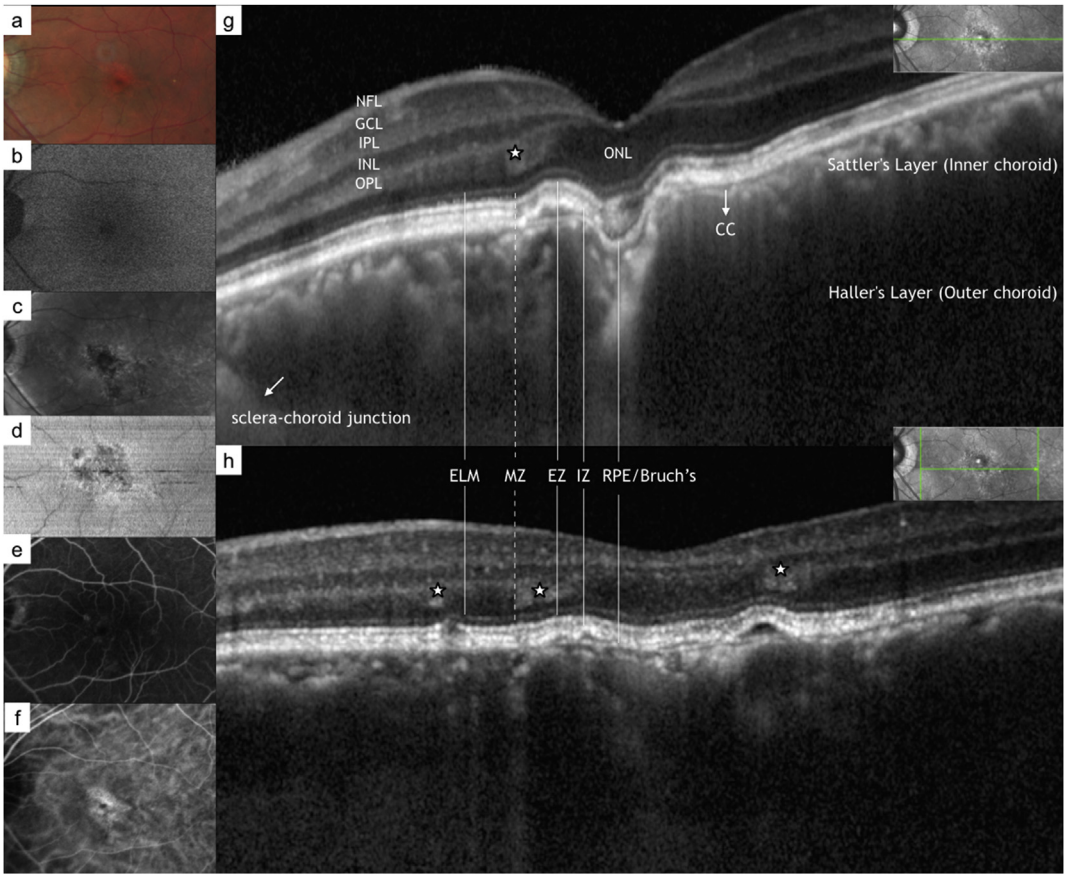

Fig. 1. Idiopathic FCE in a 51-year-old man (Case 5 OS). a. Biomicroscopic examination showed RPE mottling at the fovea. b. FAF revealed central hypo-autofluorescence. c, d. Both IR and en-face OCT showed hypo-autofluorescence at the center with surrounding irregular hyper-autofluorescence. The FCE edge was not clearly shown. e. FAG revealed multiple weak fluorescent leaking points. f. Early phase ICG showed hypo-fluorescence at the excavation with venous dilation at the edge of the FCE. g. EDI-OCT revealed a conforming, cone-shaped FCE with the irregularity of the RPE/Bruch's band, EZ, and IZ. Thicker ONL at the FCE and partial OPL thickening (asterisk) were noted. The total choroid thickness increased. The deeper choroidal vessels (Sattler's and Haller's layer) directly beneath the FCE lesion had collapsed. The choriocapillaris (CC) appeared preserved. h. EDI-OCT in a peri-FCE scan showed irregularity of the ELM, EZ, IZ and RPE/Bruch's band. Partial OPL thickening (asterisk) was also noted.

3. Results

3.1. Patients' characteristics

Ten (six male; four female) patients (12 eyes, 14 lesions) were identified in which SD-OCT scans revealed one or more focal areas of choroidal excavation. The demographic data of the patients are summarized in Table 1. In brief, all patients were ethnically Taiwanese with a mean age of 45.5 years (range, 27–74 years). The BCVA ranged from 6/12 to 6/6. All 12 eyes were myopic, and the mean spherical refractive error was −5.70 D (range, −1.5 to −11.0 D). There were no cases of myopic maculopathy or posterior staphyloma in any of the eyes with FCE. At the initial examinations, two eyes were diagnosed with CSCR, another two with idiopathic CNV, and the rest with idiopathic FCE. There were six right eyes and six left eyes. Bilateral FCE lesions were noted in two patients. One eye had two separate FCE lesions. Two patients (two eyes) were asymptomatic, six patients (six eyes) complained of gradually blurred vision, three patients (three eyes) presented with metamorphopsia, and one patient (one eye) complained of seeing flashes of light. In most patients, the presence of FCE was not clearly evident in routine clinical examinations. Funduscopy and color photography showed mild to moderate pigmentary disturbances in the corresponding area of five eyes while three of the eyes had no remarkable changes and four eyes had fundus manifestations corresponding with CSCR and CNV.

3.2. Imaging studies

3.2.1. Case 4 (Fig. 4)

This 34-year-old male reported progressive metamorphopsia in his left eye for seven years without eye trauma or any underlying disease. His BCVA was OD 6/6 OS 6/7.5 with a myopic refractive error of −10.0. The Amsler grid test showed positive results in the left eye and negative findings in the right eye. A dilated fundus examination in the left eye revealed a patch of mottling area over the fovea, and SD-OCT confirmed a subfoveal non-conforming FCE with sub-retinal fluid. The depth of the excavation was 262 μm as measured by internal caliper software with images crossing the center of

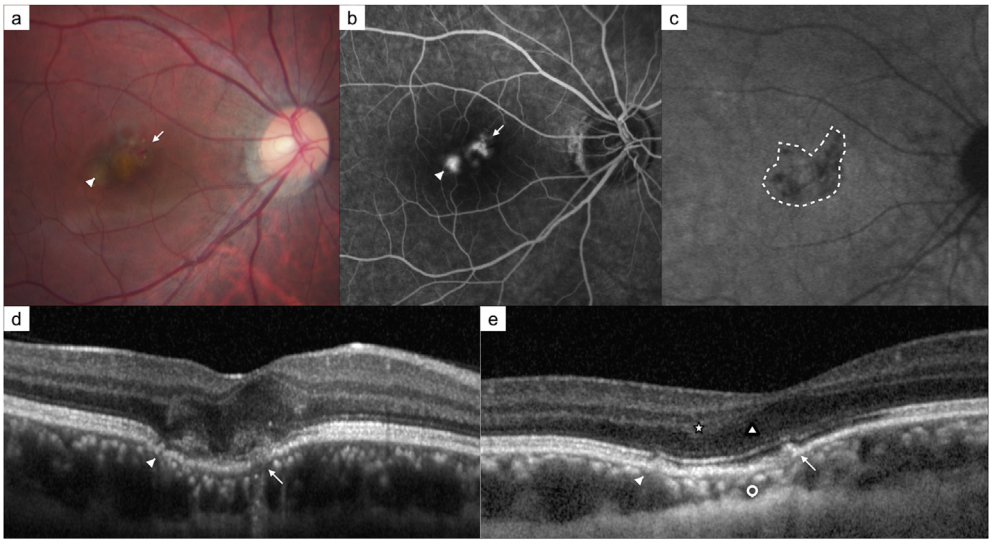

Fig. 2. FCE complicated with CNV in a 33-year-old woman (Case 1 OD). a. Biomicroscopic examination demonstrated two yellowish CNV and hemorrhage adjacent to the fovea. CNV1 (arrowhead) and CNV2 (arrow). b. FAG showed two well-defined leaking CNV lesions. c. The NIA image was taken after the resolution of CNV, and clearly showed the full extent of the FCE of hypo-autofluorescence. The FCE area on NIA was 2.84 μm^2. Regression of the CNV was no longer observed. d. SD-OCT revealed a conforming, bowl-shaped FCE and CNV with overlying retinal thickening. The irregularity of the RPE and absence of the EZ zone involved the entire FCE. e. Thirteen months after one intravitreal injection of bevacizumab, EDI-OCT showed regression of the CNV. The RPE and EZ zone smoothed out. The ONL (triangular symbol) and OPL (asterisk) appeared to be thicker over the FCE. The BCVA was 6/6, and the Amsler grid test was normal. Compression of the deeper choroidal vessels directly beneath the FCE lesions (hollow dot) and enlarged adjacent deeper choroidal vessels (Sattler's and Haller's layer) were noted. The choriocapillaris appeared to be preserved.

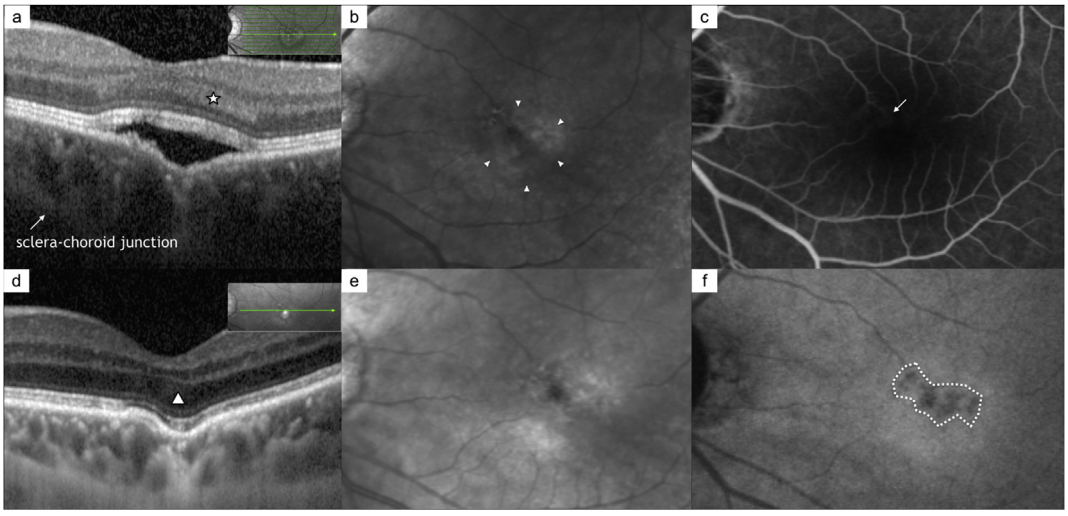

Fig. 3. FCE complicated with CSCR in a 46-year-old man (Case 3 OS). a. SD-OCT showed a non-conforming, bowl-shaped FCE with sub-retinal fluid. The OPL (asterisk) thickened. b. IR imaging revealed hypo-reflection over the FCE lesion with surrounding hyper-reflection corresponding to the SRF (arrowheads). c. FAG showed mild fluorescence leakage (arrow). d. After three years, the SRF resolved spontaneously, and the lesion became conforming FCE with the irregularity of the RPE/Bruch's band and EZ with a thicker ONL (arrowhead). The Amsler grid test showed distortion. The BCVA was 6/6.7. EDI-OCT showed that the larger caliber vessels directly beneath the FCE lesion had collapsed, and the total choroid thickness had decreased compared to the initial presentation. e. IR revealed persistent hypo-reflection over the FCE lesion with reduced surrounding reflection corresponding to the previous SRF area. f. NIA more clearly showed the full extent of the FCE and the area was 0.61 μm^2.

the excavation. The affected structures in the excavation included the RPE/Bruch's band, EZ, and ELM. The ONL over the FCE appeared to be thicker than that of the other part. EDI-OCT demonstrated deeper choroidal vessel (Haller's & Sattler's Layer) compression directly beneath the FCE lesion and enlarged choroidal vessels adjacent to the lesion. The choriocapillaris and the choroid–scleral junction appeared to be relatively unaffected. Superficial retinal layers from the retinal nerve fiber layer to the outer plexiform layer remained undisturbed. FAF imaging revealed a hypo-autofluorescent ring, and IR imaging showed hypo-reflectivity over the FCE lesion with central hyper-reflection corresponding to the SRF. Neither FAF nor IR imaging clearly showed the edge of the FCE. NIA revealed the full extent of the FCE in the left eye

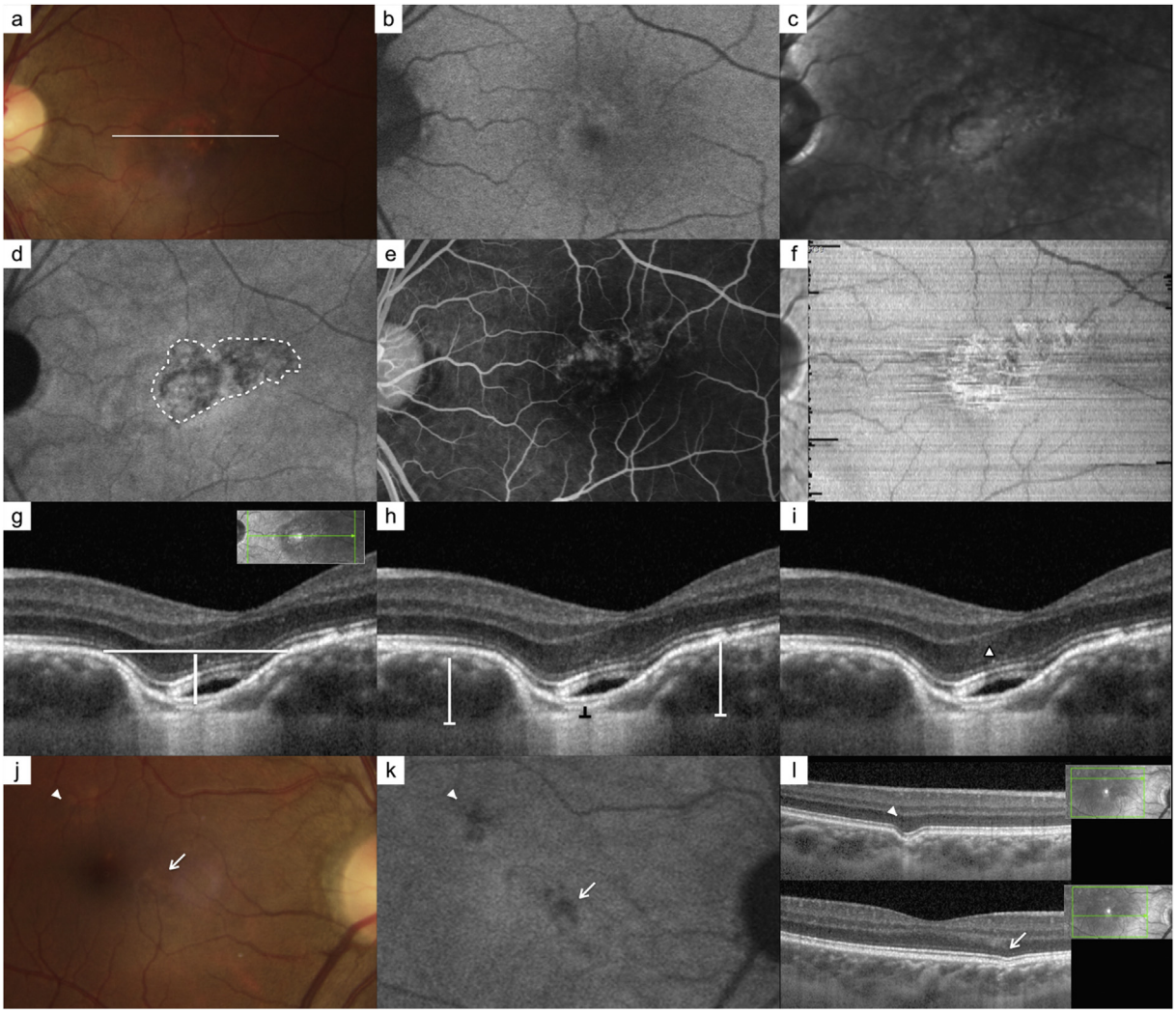

Fig. 4. FCE complicated with chronic CSCR in the left eye and idiopathic FCE in the right eye in a 33-year-old man (Case 4). a. Biomicroscopic examination demonstrated a patch of mottling area over the fovea. The white line corresponds to the section examined with SD-OCT. b. FAF revealed central hypo-autofluorescence with a hyper-autofluorescent ring which corresponded to the area of sub-retinal fluid. The FCE edge was not clear. c. IR revealed hyporeflectivity over the FCE lesion with central hyper-reflection corresponding to the SRF. The FCE edge was not clear. d. NIA showed the full extent of the FCE in the left eye. The lesion was hypo-autofluorescent. The area on NIA was 3.80 μm^2. e. FAG imaging showed multiple fluorescence leakage with discrete leaking points. f. En-face OCT revealed hyporeflectivity over the FCE lesion with surrounding hyper-reflection. The border was not clearly shown. g. SD-OCT showed a non-conforming FCE with sub-retinal fluid. The depth of the excavation was 262 μm measured by internal caliper software with images crossing the center of the excavation. h. The choroid was thinned out at the area of the FCE. The choroidal thickness under FCE was 43 μm. The ratio of the thickness of the choroid under the FCE to the unaffected sites near the excavation was 0.14 = 43/[(293 + 344)/2]. Compression of the deeper choroidal vessels (Haller's & Sattler's Layer) directly beneath the FCE lesion. The adjacent outer choroidal vessels appeared to be enlarged. The choriocapillaris and sclero-choroidal junction appeared to be relatively unaffected. i. The affected structures in the excavation generally included the RPE/Bruch's band, EZ and ELM. The ONL (triangular symbol) overlying the excavation appeared to be thicker than that of the other part. The ONL thickness (ONLt) was 123 μm. j. Biomicroscopic examination of the right eye showed two mild RPE mottling areas at the peri-fovea. k. NIA of the right eye showed two hypo-fluorescent lesions. Although the patient denied any symptoms in the right eye, due to positive findings on NIA imaging we rechecked SD-OCT which revealed two small FCE lesions corresponding to the NIA image. l. EDI-OCT of temporal upper and nasal lower lesion scans showed two conforming, cone-shaped FCE lesions with irregularity of EZ and RPE/Bruch's band.

with hypo-autofluorescence and the area on NIA was 3.80 μm^2. NIA also showed two hypo-fluorescent lesions in the right eye. Although the patient denied any symptom in the right eye, due to positive findings on the NIA image we rechecked SD-OCT, which revealed two small, conforming FCE lesions corresponding to the NIA image. FAG showed multiple fluorescence leakage with discrete leaking points in the left eye and mild fluorescence leakage in the right eye.

3.2.2. Spectral-domain optical coherence tomography, enhanced depth imaging optical coherence tomography, and multidimensional en-face optical coherence tomography findings

In all patients, SD-OCT imaging was necessary to detect FCE (Table 2). The FCE had a subfoveal location in 11 lesions, a para-foveal location in one lesion, and a perifoveal location in two lesions. The affected structures in the

Table 1
Demographic data of the patients with focal choroidal excavation.

Case	Eye	Lesion	R/L[a]	Age/sex (M/F[b])	Symptoms	BCVA[c]	SE[d]	Amsler grid	Complication
1	1	1	R	33/F	Metamorphopsia	6/12	−8.5	0	CNV[g]
2	2	2	R	43/F	Blur	6/7.5	−4	0	CNV
3	3	3	L	46/M	Seeing flash	6/6.7	−8	6	CSCR[h]
4	4	4	R, TU[e]	33/M	Asymptomatic	6/6	−11.0	0	Idiopathic
		5	R, NL[f]						
	5	6	L		Metamorphopsia	6/7.5	−11.0	40	CSCR
5	6	7	L	51/M	Blur	6/10	−5.5	NA[i]	Idiopathic
6	7	8	L	52/M	Blur	6/7.5	−5.5	NA	Idiopathic
7	8	9	L	74/M	Blur	6/8.5	−3.0	NA	Idiopathic
8	9	10	R	27/M	Blur	6/7.5	−6.5	0	Idiopathic
9	10	11	R	40/F	Blur	6/6	−1.5	5	Idiopathic
10	11	12	R, TU	56/F	Asymptomatic	6/6	−2.5	0	Idiopathic
		13	R, Central						
	12	14	L		Metamorphopsia	6/10	−2.5	34	Idiopathic

[a] R/L = right/left.
[b] M/F = male/female.
[c] BCVA = best-corrected visual acuity.
[d] SE = spherical equivalent.
[e] TU = temporal upper.
[f] NL = nasal lower.
[g] CNV = choroidal neovascularization.
[h] CSCR = central serous chorioretinopathy.
[i] NA = not applicable.

Table 2
Findings of 14 FCE in 12 eyes on SD-OCT, EDI-OCT and near-infrared autofluorescence imaging.

Case	Eye	Lesion	Location	Depth (μm)	NIA area (μm^2)	Volume[a] (μm^3)	OPLt[b] (μm)	ONLt[c] (μm)	CT[d] under FCE (μm)	CT ratio[h]	Choriocapillaris	Haller's & Sattler's layer	CO[e]/NC[f]	Types (B/C/M)[g]
1	OD	1	Fovea	162	2.84	153.36	45	69	94	0.37	N[j]	Collapse	CO	B
2	OD	2	Fovea	164	1.27	69.43	0	59	83	0.36	N	Collapse	NC	M
3	OS	3	Fovea	107	0.61	21.76	20	91	155	0.62	Collapse	N	CO	M
4	OD	4	Peri-fovea	109	0.42	15.26	34	96	78	0.24	N	Collapse	CO	C
		5	Peri-fovea	46	0.32	4.91	31	99	227	0.88	N	N	CO	B
	OS	6	Fovea	262	3.80	331.87	28	123	43	0.14	Collapse	Collapse	NC	M
5	OS	7	Fovea	138	NA[i]	NA	0	122	403	0.69	Collapse	Enlarge	NC	C
6	OS	8	Fovea	118	NA	NA	16	87	63	0.33	N	Collapse	CO	M
7	OS	9	Fovea	116	NA	NA	29	91	29	0.18	N	Collapse	CO	M
8	OD	10	Fovea	88	0.32	9.39	91	18	268	0.84	Collapse	Enlarge	CO	B
9	OD	11	Fovea	188	0.60	37.6	0	91	49	0.17	N	Collapse	NC	C
10	OD	12	Para-fovea	70	0.05	1.17	35	88	168	0.75	N	Collapse	CO	B
		13	Fovea	126	0.42	17.64	17	145	86	0.34	N	Collapse	CO	M
	OS	14	Fovea	297	1.15	113.85	65	127	52	0.17	Collapse	Collapse	CO	M
Average				142.2	1.07	70.57	29.36	93.26	128.43	0.43				
Standard deviation				69.38	1.89	99.6	25.39	31.71	106.72	0.27				

[a] Volume = NIA area × Depth × 1/3.
[b] OPLt = outer plexiform layer thickness.
[c] ONLt = outer nuclear layer thickness.
[d] CT = choroidal thickness.
[e] CO = conforming.
[f] NC = non-conforming.
[g] B/C/M = bowl/cone/mixed.
[h] CT ratio = the ratio of the thickness of the choroid under the FCE to the unaffected sites near the excavation.
[i] NA = not available.
[j] N = normal.

excavation included the RPE-Bruch's band, EZ, ELM, ONL, and OPL. In 13 of the 14 lesions, the excavation involved the ONL, which also appeared to be thicker than that of the other part (Figs. 1–4). Partial thickening of the OPL was also noted in 13 lesions (Figs. 1–3). The average depth was 142.2 μm (range 46–297 μm).

The EDI-OCT allowed us to study the choroidal structures and scleral contours in details. The choroid was thinned out at

the bottom of the FCE, and the average thickness of the choroid was 128.43 μm (range 29–403 μm). The ratio of the thickness of the choroid under the FCE to the unaffected sites near the excavation was 0.43 (range, 0.14–0.88). None of the eyes showed any staphyloma of choroid–scleral bands on the OCT scan, and the choroidal–scleral interface was smooth in all 12 eyes.

Due to current limitations in technology, manual adjustments of the precise line were needed in each en-face OCT image in the measurement of FCE area. The precise FCE area cannot be obtained.

3.2.3. Fundus autofluorescence, near-infrared autofluorescence and infrared reflectance findings

FAF showed hypo-autofluorescence in FCE lesions (Figs. 1 and 4), but was relatively unremarkable compared with NIA imaging. FAF showed that the area corresponding to the CNV (case 1) or sub-retinal fluid (case 4) (Fig. 4) was hyper-autofluorescent. During the follow-up period, the center of the lesion was relatively hypo-autofluorescent after the CNV had regressed. After resolution, the FCE lesion was unremarkable in FAF.

The FCE in IR imaging appeared to be heterogeneous and hypo-reflective (Figs. 1, 3 and 4). However, in two cases (case 4 OD, case 10 OD), the FCE lesions were not successfully detected by IR. In cases with CNV (cases 1 and 2), IR revealed hyper-reflectivity that corresponded to the CNV and hypo-reflectivity on FCE. During regression of the CNV, IR became less hyper-reflective corresponding to the CNV. In cases with CSCR (cases 3 and 4), IR imaging revealed hypo-reflection over the FCE lesion with surrounding hyper-reflection corresponding to the SRF (Fig. 3). During regression of the SRF, IR imaging showed persistent hypo-reflection over the FCE lesion with decreased surrounding reflection corresponding to the previous area of sub-retinal fluid.

In areas where the choroid started to excavate as shown in SD-OCT, hypo-autofluorescence in NIA was noted (Figs. 2–4). The area of hypo-fluorescence in NIA of all the FCE lesions showed good correlation with the size. The average area of the FCE on the NIA image was 1.07 μm^2 (range 0.05–3.80 μm^2). We calculated the volume of FCE using the formula for triangular pyramid volume (area measured by NIA image multiplied by the depth measured by SD-OCT × 1/3), and the average volume was 70.57 μm^3 (range 1.67–331.87 μm^3).

The area of FCE was associated with complications ($p = 0.014$) and the volume (NIA area × Depth measured by SD-OCT × 1/3) was associated with subjective distortion ($p = 0.051$, Spearman's correlation = 0.600).

3.2.4. Fluorescein angiography and indocyanine green angiography findings

FAG was performed in four eyes of four patients (case 1 with CNV, cases 3 and 4 with CSCR, case 5 with IFCE) (Figs. 1–4). The image showed varying degrees of hyper-fluorescence and hypo-fluorescence related to a range of RPE changes or blocked fluorescence due to CNV, hemorrhage or subretinal fluid over the FCE. ICGA was performed in two patients (cases 5 and 8 with IFCE) (Fig. 1) and showed hypo-fluorescence at the excavation, with venous dilation noted at the edge of the FCE. Abnormal staining was found on ICGA in the late phase. However, neither the increase nor the decrease of fluorescence in FAG or ICGA correlated with the edge of the FCE.

4. Discussion

To our best knowledge, this is the pilot study on different modalities in screening and monitoring of FCE and we found that NIA was the most sensitive tool in area measurement and peripheral lesion detection. We also discovered a strong correlation between area of FCE and complication and it might provide a hint for subsequent healthcare from clinical perspective.

4.1. Etiology and pathologic mechanism of focal choroidal excavation

Several primary etiologic and pathologic mechanisms have been reported for FCE including congenital, inflammation, infection or aberrant choroidal circulation. Similar to previous reports on the congenital mechanism,[2,20] the patients in the current study had no family history or any related ocular disease. The clinical courses were stable, and all patients had a BCVA better than 6/12. Faulty differentiation of the chorioretinal or typical choroidal coloboma has been proposed.[2] Choroidal excavation involves the RPE, choriocapillaris, and photoreceptors in the fovea or perifoveal region.[1,5,6,21] We observed a thickened, attenuated or irregular RPE-Bruch's band and EZ. Thickening of the ONL was noted in almost every FCE lesion (Figs. 1–4). A possible mechanism is that with a small defect at the choroid, adhesion between the RPE and the photoreceptors that normally keeps them attached could pull the retina outward. The inner retina or the vascular system may attempt to hold the retina in place. These two forces may result in ONL thickening.[4,22] Partial thickening of the OPL following the contour of the excavation in the current study (13 lesions in 11 eyes) and a previous report[2] were also noted. We hypothesize that the OPL thickening observed on SD-OCT (Figs. 1–3) was due to reflectivity changes associated with macular pathology.[23] Layers from the INL to RNFL were relatively normal in the current study, consistent with previous reports.[6,24]

Inflammation and infection have also been proposed to be possible etiologies. The thinned-out choroidal tissue and complications such as CSCR or CNV seen in the current study and others may represent an inflammation-related mechanism.[6,14,21,25]

With regards to the aberrant choroidal circulation mechanism, the hypo-fluorescence at the FCE, hyper-fluorescence around the excavation in ICGA and collapsed large choroid vessels may indicate aberrant choroidal circulation in our cases as suggested in other reports.[5–7,10,21,24] The choroid choriocapillaris under the FCE appeared to be relatively

normal while the deeper choroidal vessels had collapsed (Haller's & Sattler's layer).

The cause of the excavation may be multifactorial, and further studies with longer-term follow-up are needed to monitor changes in the depth of FCE and choroidal vessels.

4.2. Different modalities in detection of focal choroidal excavation

FAF has been shown to originate from lipofuscin distribution in the outer segment of photoreceptors and the RPE. IR is reflected by the inner limiting membrane, retinal nerve fiber layer, retinal photoreceptor layer, RPE, choroid, and sclera level. IR provides better visualization of the subretinal and choroidal structures. NIA is thought to originate from melanin,[16] a fluorophore present in the RPE cells and choroid, or compounds closely related to melanin (oxidized melanin, melanolipofuscin). In normal eyes, due to increased melanin in the RPE at the fovea, high autofluorescence centered on the foveal is noted on NIA imaging. Several retinal and choroidal disorders including age-related macular degeneration, choroidal nevus, CSCR, and CNV have been recorded by NIA.[17−19]

In the current study, NIA offered unique imaging of the extent of FCE lesions as revealed by hypo-autofluorescence. In the FCE lesions, the underlying choroid was thinner, and the amount of melanin decreased compared to the other normal-thickness choroid, compatible with the NIA results. In areas where focal choroid had started to excavate as shown in SD-OCT, there was hypo-autofluorescence in NIA, and it was a more specific imaging tool in defining the margin of FCE than IR, FAF, ICGA, and FA. Although en-face OCT and NIA both provided the data of FCE area, NIA image showed the area margins more clearly and did not need manual adjustments of the layer line which was needed in en-face OCT. We also found that eyes with maculopathy such as CNV and CSCR were associated with greater FCE area and the volume of FCE was associated with subjective distortion.

As for the detection for FCE lesion, in cases with bilateral involvement or multiple lesions in one eye, SD-OCT of the fovea may not detect all lesions especially when the lesion is more peripheral. However, NIA image could detect all lesions at one time (Fig. 4).

Therefore, SD-OCT provided morphological characteristics and NIA provided FCE area data precisely and detected lesion efficiently. Using the combination of NIA and SD-OCT could help in detecting FCE lesion and decrease the missing rates. Both modalities were noninvasive, rapid image acquisition and feasible to perform at each clinical visit.

4.3. Study limitations

Limitations of the current study include limited case numbers and short follow-up period. However, we found that the volume of FCE was associated with subjective distortion while the area was associated with complications.

In conclusion, recording the area and volume of FCE help in monitoring patients for the potential development of other retinal diseases. The combination of non-invasive SD-OCT and NIA in patients with deeper chorioretinal abnormalities is recommended and is helpful for patients with FCE to monitor its progression, visual acuity, and functional status.

Acknowledgments

We acknowledge Yei-Ching Chen, Cheng Hsin General Hospital for his great help on data collection and Han-Chung Liu, Taipei Veterans General Hospital for her great help on data collection.

References

1. Jampol LM, Shankle J, Schroeder R, Tornambe P, Spaide RF, Hee MR. Diagnostic and therapeutic challenges. *Retina* 2006;**26**:1072−6.
2. Liu GH, Lin B, Sun XQ, He ZF, Li JR, Zhou R, et al. Focal choroidal excavation: a preliminary interpretation based on clinic and review. *Int J Ophthalmol* 2015;**8**:513−21.
3. Shinojima A, Kawamura A, Mori R, Yuzawa M. Morphologic features of focal choroidal excavation on spectral domain optical coherence tomography with simultaneous angiography. *Retina* 2014;**34**:1407−14.
4. Guo J, Zhong L, Jiang C, Zhou X, Xu G, Wang W, et al. Clinical and optic coherence tomography findings of focal choroidal excavation in Chinese patients. *BMC Ophthalmol* 2014;**14**:63.
5. Obata R, Takahashi H, Ueta T, Yuda K, Kure K, Yanagi Y. Tomographic and angiographic characteristics of eyes with macular focal choroidal excavation. *Retina* 2013;**33**:1201−10.
6. Margolis R, Mukkamala SK, Jampol LM, Spaide RF, Ober MD, Sorenson JA, et al. The expanded spectrum of focal choroidal excavation. *Arch Ophthalmol* 2011;**129**:1320−5.
7. Katome T, Mitamura Y, Hotta F, Niki M, Naito T. Two cases of focal choroidal excavation detected by spectral-domain optical coherence tomography. *Case Rep Ophthalmol* 2012;**3**:96−103.
8. Kobayashi W, Abe T, Tamai H, Nakazawa T. Choroidal excavation with polypoidal choroidal vasculopathy: a case report. *Clin Ophthalmol* 2012;**6**:1373−6.
9. Ellabban AA, Tsujikawa A, Ooto S, Yamashiro K, Oishi A, Nakata I, et al. Focal choroidal excavation in eyes with central serous chorioretinopathy. *Am J Ophthalmol* 2013;**156**:673−83.
10. Xu H, Zeng F, Shi D, Sun X, Chen X, Bai Y. Focal choroidal excavation complicated by choroidal neovascularization. *Ophthalmology* 2014;**121**:246−50.
11. Lee JH, Lee WK. Choroidal neovascularization associated with focal choroidal excavation. *Am J Ophthalmol* 2014;**157**:710−8. e1.
12. Say EA, Jani PD, Appenzeller MF, Houghton OM. Focal choroidal excavation associated with polypoidal choroidal vasculopathy. *Ophthalmic Surg Lasers Imaging Retina* 2013;**44**:409−11.
13. Lee CS, Woo SJ, Kim YK, Hwang DJ, Kang HM, Kim H, et al. Clinical and spectral-domain optical coherence tomography findings in patients with focal choroidal excavation. *Ophthalmology* 2014;**121**:1029−35.
14. Lim FP, Loh BK, Cheung CM, Lim LS, Chan CM, Wong DW. Evaluation of focal choroidal excavation in the macula using swept-source optical coherence tomography. *Eye (Lond)* 2014;**28**:1088−94.
15. Luk FO, Fok AC, Lee A, Liu AT, Lai TY. Focal choroidal excavation in patients with central serous chorioretinopathy. *Eye (Lond)* 2015;**29**:453−9.
16. Keilhauer CN, Delori FC. Near-infrared autofluorescence imaging of the fundus: visualization of ocular melanin. *Invest Ophthalmol Vis Sci* 2006;**47**:3556−64.
17. Skondra D, Papakostas TD, Hunter R, Vavvas DG. Near infrared autofluorescence imaging of retinal diseases. *Semin Ophthalmol* 2012;**27**:202−8.
18. Weinberger AW, Lappas A, Kirschkamp T, Mazinani BA, Huth JK, Mohammadi B, et al. Fundus near infrared fluorescence correlates with fundus near infrared reflectance. *Invest Ophthalmol Vis Sci* 2006;**47**:3098−108.

19. Toju R, Iida T, Sekiryu T, Saito M, Maruko I, Kano M. Near-infrared autofluorescence in patients with idiopathic submacular choroidal neovascularization. *Am J Ophthalmol* 2012;**153**:314−9.
20. Abe S, Yamamoto T, Kirii E, Yamashita H. Cup-shaped choroidal excavation detected by optical coherence tomography: a case report. *Retin Cases Brief Rep* 2010;**4**:373−6.
21. Ellabban AA, Tsujikawa A, Matsumoto A, Yamashiro K, Oishi A, Ooto S, et al. Three-dimensional tomographic features of dome-shaped macula by swept-source optical coherence tomography. *Am J Ophthalmol* 2013;**155**:320−8.
22. Kumano Y, Nagai H, Enaida H, Ueno A, Matsui T. Symptomatic and morphological differences between choroidal excavations. *Optom Vis Sci* 2013;**90**:e110−8.
23. Lujan BJ, Roorda A, Knighton RW, Carroll J. Revealing Henle's fiber layer using spectral domain optical coherence tomography. *Invest Ophthalmol Vis Sci* 2011;**52**:1486−92.
24. Wakabayashi Y, Nishimura A, Higashide T, Ijiri S, Sugiyama K. Unilateral choroidal excavation in the macula detected by spectral-domain optical coherence tomography. *Acta Ophthalmol* 2010;**88**:87−91.
25. Savastano MC, Rispoli M, Di Antonio L, Mastropasqua L, Lumbroso B. Observed positive correlation between Epstein−Barr virus infection and focal choroidal excavation. *Int Ophthalmol* 2014;**34**:927−32.